STATE-OF-ART Nb-BEARING COLD-ROLLED STEEL SHEET FOR AUTOMOTIVE APPLICATION

Toshiaki Urabe, Yoshihiko Ono, Takeshi Fujita, Yuji Yamasaki and Yoshihiro Hosoya

JFE Steel Corporation; 1, Kawasaki-cho, Chuo-ku; Chiba 260-0835, Japan

Keywords: IF steel, high strength steel, grain refinement, precipitate-free zone (PFZ).

Abstract

A new type of IF cold-rolled high strength steel (HSS) with strength levels of 390 and 440 MPa has been developed using the chemistry of extra-low carbon steel containing around 60 ppm C with an intentional addition of niobium by hybridizing the precipitation hardening with niobium carbides and the supplemental solid-solution hardening. In this steel, the formation of PFZ (Precipitation Free Zones) in the neighborhood of grain boundaries is the most typical micro-structural feature responsible for the unique mechanical properties described as follows:
1) The yield strength hardly increases by the existence of PFZ even when grain refinement is taking place.
2) An outstanding high Lankford value is obtained under the fine grain structure.
3) The secondary-work embrittlement resistance is improved by not only the grain refinement but also the existence of PFZ.
4) A sufficiently good surface quality is achieved for galvannealed sheet.
Principles of the unique mechanical properties of the steel have been revealed based on the sub-structure formation during continuous annealing. The results of a further approach to improve these as a state-of-the-art product being widely used for the exposed panels in the body-in-white are introduced in the paper.

Introduction

Niobium (Nb) is an effective element to control the microstructure in both hot-rolled and cold-rolled steel sheets being widely used for the automotive parts. The main purpose of the Nb addition in the interstitial free (IF) steels for deep-drawing quality cold-rolled steel sheets is to refine the microstructure in the hot band through retardation and recrystallization by both the solute-drag of niobium and the pinning of fine precipitates of NbC during the hot-rolling process. This result brings a positive effect to promote the nucleation and the growth of the γ-fiber texture, <111>//ND after cold-rolling followed by continuous annealing. Another advantage of Nb additions to IF steel is that it does not deteriorate the hot-dip galvanizability as compared to titanium (Ti) in view of the homogeneous surface appearance of exposed panels.

The sheet steels for automotive exposed panels such as side-panels and fenders are required to possess excellent press-formability, such as deep-drawability and stretch-formability, as well as low surface reflection after press forming. In order to satisfy these requirements, IF steels, in which carbon and nitrogen contents are reduced to less than 30 ppm and Nb and Ti are added to eliminate solute carbon and nitrogen, have been widely adopted. During the 1990s, these IF steels exhibit excellent Lankford values, typically above 1.5, and high elongations that contribute to the weight reduction of the body-in-white enabling a one-piece side panel through the improvement of the deep-drawability. The cold-rolled high strength steel sheets (HSS) with

deep-drawing quality have been developed based on the IF steel by alloying solid-solution strengthening elements such as silicon, phosphorous and manganese in the last decades [1]. Such grades were commercialized with a tensile strength of up to 440 MPa. However, the increase in the contents of these solid-solution elements deteriorates the mean r-value and cause both a higher yield strength and yield ratio leading to a decrease of the n-value and a deterioration of the surface reflection in the exposed panel. When an IF steel is strengthened by solid-solution elements, the difference between intra-granular and inter-granular strength is enhanced leading to a higher transition temperature for secondary-work-embrittlement [2]. In the case of widely applied galvannealed steels,, another critical issue for the product application in exposed panels is to qualify the uniform coated surface appearance by eliminating the addition of silicon.

In this study, grain refinement and precipitation hardening are combined with solid-solution hardening in IF-HSS to improve the mechanical properties for press forming and the anti-secondary work embrittlement of IF-HSS. The metallurgical background leading to the unique mechanical properties and advantages of these newly developed IF-HSS applied to automotive exposed panels are verified in the try-out-press for the exposed panel.

Alloy Design of Grain-refined IF-HSS

Conventional IF-HSS is strengthened by adding solid-solution elements such as silicon, manganese and phosphorous to a mild IF steel with around 270 MPa in tensile strength as shown in Figure 1. In the new grain-refined IF-HSS, according to Figure 1, the carbon content in the steel is three times as much as that in the conventional IF steel, and niobium is added above the stoichiometric ratio to carbon giving not only an interstitial free chemistry in the steel, but also dispersing a higher amount of fine niobium carbo-nitrides. These fine precipitates increase the tensile strength by both, grain refinement and precipitation hardening. Therefore, the total amount of solid-solution elements can be reduced compared with those in the conventional IF-HSS, which is desirable in view of the uniform surface appearance of the galvannealed steel. Grain refinement is an effective method to improve the secondary work embrittlement, but is a restriction for the application of IF-HSS.
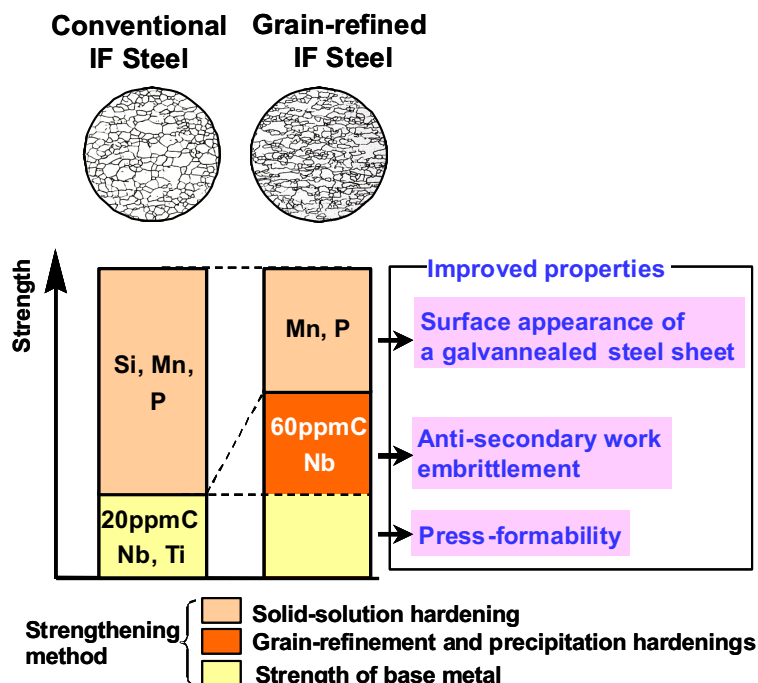

Figure 1. Schematic diagram showing the metallurgical concept of the newly developed steel compared to the conventional IF steel.

410

Comparison in Mechanical Properties

Experimental procedure

Materials with the chemical compositions listed in Table I were melted and cast in the laboratory. Steel A shows the chemical composition of a typical conventional ultra low carbon niobium bearing IF steel, where the atomic ratio of carbon and niobium, (Nb/C) is higher than 1.0. In steel B, the carbon and niobium content is much higher than that in steel A to increase the tensile strength by NbC precipitates.

Table I. Chemical compositions of steels. (mass%).

Steel	C	Si	Mn	P	N	Nb	Nb/C
A	0.0020	0.02	0.66	0.043	0.0029	0.022	1.42
B	0.0052	0.01	0.62	0.040	0.0032	0.068	1.69

Nb/C: Atomic ratio of niobium against carbon contents.

The ingots were hot-rolled to an intermediate size of 30 mm gauge. After soaking at 1200ºC for one hour, they were hot-rolled to 2.8 mm gauge with a finishing temperature of 900ºC followed by air-cooling. In order to simulate the hot coiling, hot bands were soaked at 640ºC for one hour followed by furnace cooling. After pickling, the hot-bands were cold-rolled to 0.56 mm gauge with a rolling reduction of 80%. These cold-rolled sheets were annealed at different temperatures such as 830, 850 and 870ºC for 50 seconds using a salt bath and subsequently subjected to skin-pass rolling with an elongation of 0.7%. Tensile tests were carried out using JIS No.5 specimens cut in the transverse direction of the sheet whose gauge width and gauge length is 25 and 50 mm, respectively. The r-values were measured at 15% strain in three directions being 0°, 45° and 90° to the rolling direction and the mean r-value was estimated by the following equation:

$$\text{mean-r} = [r(0°) + 2r(45°) + r(90°)]/4 \qquad (1)$$

The recrystallization behavior during annealing was examined by estimating the change in hardness measured at the center thickness of the specimen's cross section annealed in the range from 600 to 870ºC. The texture change during recrystallization was evaluated by normalized relative values of integrated X-ray intensities of the {111}, {100} and {211} planes. The {100}, {100} and {211} pole figures were measured in the annealed specimens at 850ºC. Hence, all of the textures were measured in the middle of the thickness. The $\varphi_2=45º$ sections of the orientation distribution functions, ODFs were also calculated in the annealed specimens by the series expansion method ($l_{max.} = 22$) from the complete pole figures of {111}, {100} and {211} planes. Microstructures were observed with the optical microscope and the grain size was measured by the point-counting method. The distribution of fine precipitates in the annealed specimens was observed by TEM using replicas.

Recrystallization behavior

Figure 2 shows the effects of carbon and niobium contents on the hardness change with the annealing temperature. Recrystallization in steel B containing higher amounts of carbon and niobium starts at higher temperature than in steel A. The recrystallization finishing temperatures, T_R of steel A and B are 680ºC and 740ºC, respectively. Steel B recrystallizes 60ºC higher than steel A. Optical micrographs of steel A and B after annealing at 850ºC are shown in Figure 3. The ferrite grain size of steel B is refined down to 9 μm compared to that of steel A being 13 μm.
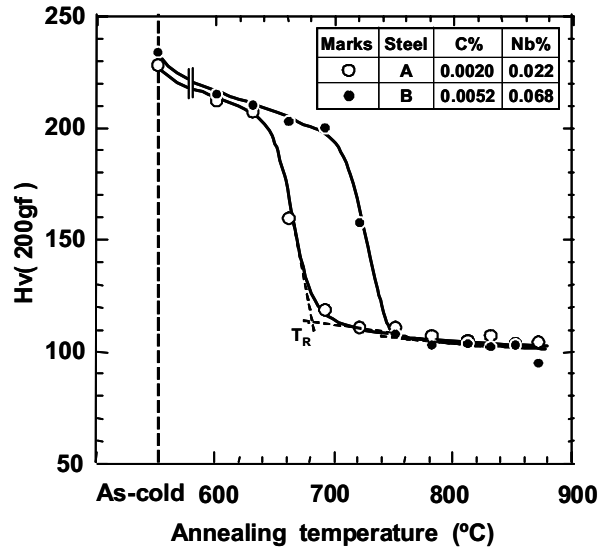
Figure 2. Change in hardness during annealing in cold-rolled samples of steel A and steel B.

Mechanical properties

The mechanical properties of annealed sheets at 830 to 870°C are shown in Figure 4. The increment in tensile strength, ΔTS of steel B against steel A is approximately 30 MPa at each temperature. It is inferred that the tensile strength of steel B was increased by precipitation hardening and grain refinement. However, the yield ratio in steel B is 10% lower than that in steel A. If these two strengthening mechanisms increase the tensile strength of steel B, the yield ratio should be also increased with the increase in yield stress. Therefore, it is inferred that this apparently inconsistent behavior was caused by a different yielding mechanism.
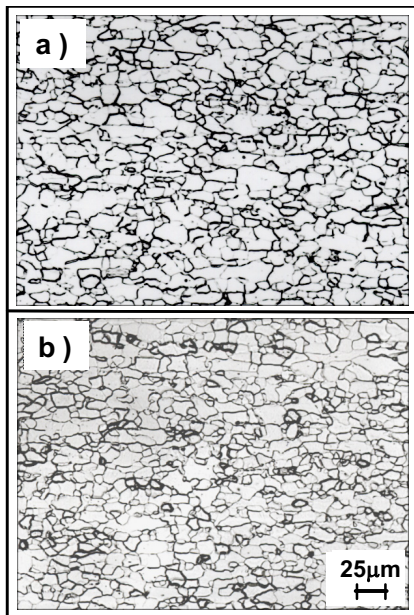

Figure 3. Optical micrographs in the cross-section of the annealed samples at 850 °C of steel A (a) and steel B (b).
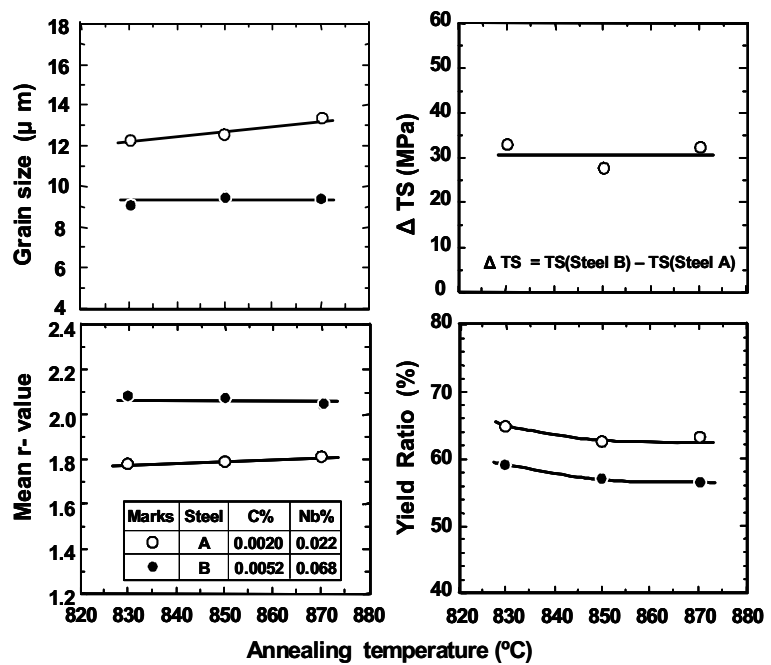
Figure 4. Comparison of the mechanical properties of the developed steel B with those of the conventional steel A.

412

The mean r-value of steel B being 2.0 is 0.2 higher than that of steel A. It is inferred that higher amounts of carbon and niobium in excess of the stoichiometric ratio of niobium to carbon leads to the improved recrystallization texture. Accordingly, the texture changes during recrystallization were investigated in both steels.

Mechanism of Improvement in the Lankford Value of Grain-Refined IF-HSS [4]

The mean r-value in steel sheets is strongly related to the crystallographic orientation and the materials having a higher volume fraction of grains with {111} planes facing to the sheet surface, <111>//ND, and lower amounts of {100} plane, <100>//ND, show higher mean r-values. This crystallographic orientation distribution, called texture, is determined by the final annealing process in the commercial production of sheet steels.

Changes in the integrated X-ray intensity ratios for {111} and {100} planes with the progress of recrystallization during annealing are shown in Figure 5. In the textures of the cold-rolled specimens, significant differences in the two components between both steels were not observed. However, the recrystallization texture of steel B is markedly improved to a more favorable r-value with the progress of recrystallization, where the <111>//ND grains increased and the <100>//ND grains decreased. The $\varphi_2 = 45°$ sections of the orientation distribution functions in the annealed specimens at 850ºC are shown in Figure 6. In both steels, the <111>//ND fiber is fully developed and the main orientation is close to {111}<112>. In contrast to steel A, the distribution around the <111>//ND in steel B is narrower and its intensity is stronger.

The difference in the texture change between both steels is that the <111>//ND grains in steel B significantly increase with the progress of recrystallization despite of almost identical intensities of the {111} and {100} grains in the cold-rolled textures. This indicates that the growth rate of the <111>//ND nuclei per unit volume in steel B is faster than that in steel A leading consequently to both, the lower volume fractions of the <100>//ND grains consumed by the <111>//ND grains as shown in Figure 5 and the stronger <111>//ND fiber profiles as shown in Figure 6.

Figure 7 shows optical micrographs of hot-band cross-sections of steels A and B. The mean ferrite grain size of steel B being about 11µm is smaller than that of steel A being about 14 µm. It is inferred that the fine ferrite structure in the hot band of steel B is caused by the γ to α transformation from both, the deformed austenite and the fine recrystallized austenite grains accompanied with the retardation of the austenite recrystallization during hot rolling.

It has been reported that the grain boundary in the hot-band is a favorable nucleation site for the ND//<111> grains during recrystallization at annealing. The hot-band ferrite grain in steel B is smaller than that in steel A and the grain boundary area in steel B is 27% larger than that in steel A, provided that the grain shape is spherical. Therefore, the larger number of the <111>//ND recrystallized grains in steel B, which nucleate in the vicinity of the grain boundaries of the hot band, can provide the large grain boundary area to grow into the deformed matrix even under the same migration rate to steel A.
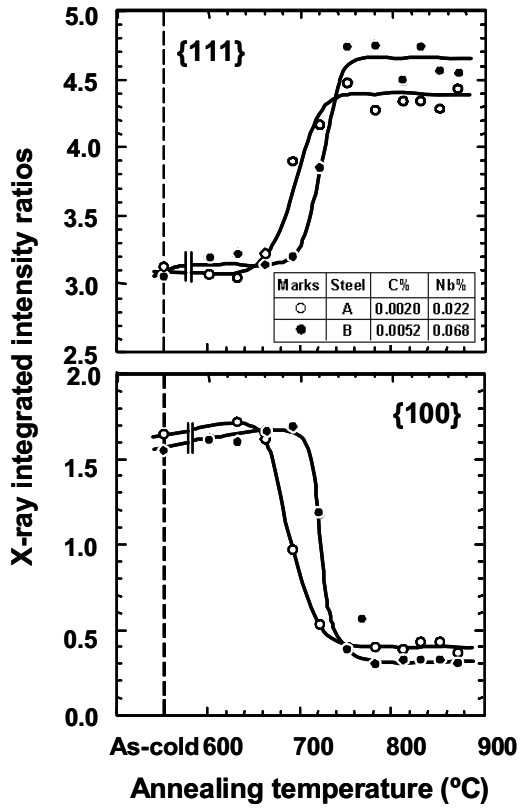
Figure 5. Changes in normalized X-ray integrated intensity ratios of {111} and {100} planes with annealing temperature.
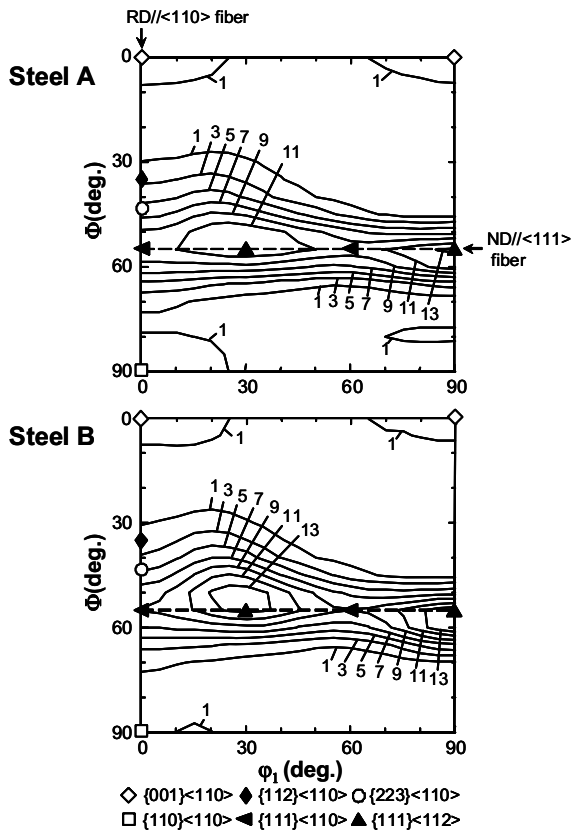
Figure 6. φ₂=45º sections of the ODFs in the samples annealed at 850ºC in steel A and steel B, respectively.
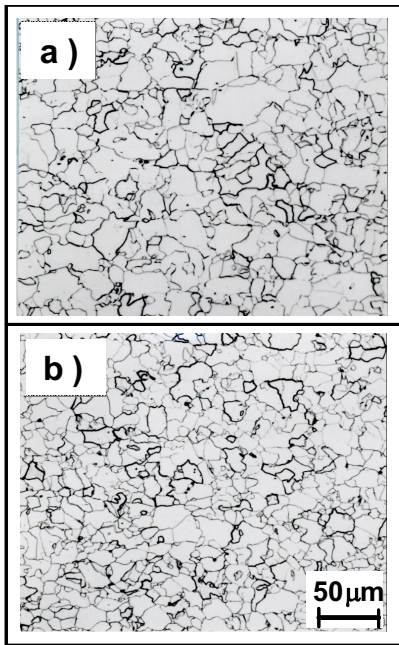

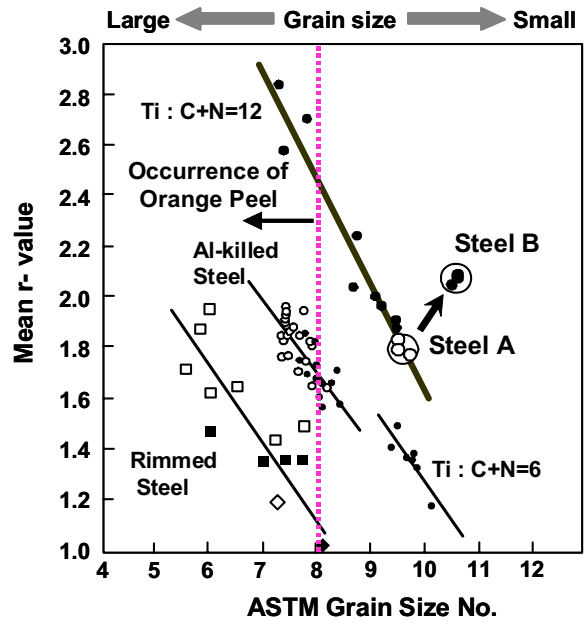Figure 7. Optical micrographs in the cross-section of the hot bands of steel A (a) and steel B (b).

Figure 8. Correlation between ASTM grain size numbers and mean r-values of cold-rolled steel sheets.

Generally, the mean r-value can be improved by elevating the annealing temperature because of the preferential grain growth of the {111} grains and can attain values above 2.5 by using IF steel as shown in Figure 8 [6]. However, the steel sheets with coarse grains cause a rugged surface after press forming, the so-called "orange-peel", which is not suitable for the surface quality of the exposed panel. Although the correlation between the mean r-value and the grain size number in case of steel A corresponds to that of titanium bearing IF steel, steel B having a fine grain structure exhibits the more desirable relationship between mean r-value and grain size than the conventional IF steels with regard to practical applications.

Mechanism of Lower Yielding in Grain-Refined IF-HSS [4]

Although it is well known that both grain-refinement and precipitation hardening are the strengthening methods by which the yield ratio is increased, the grain-refined IF-HSS investigated in this study exhibited a lower yield ratio compared to the conventional solid solution hardened IF-HSS, which is inconsistent with the conventional experience. Therefore, the precipitation behavior after annealing in steel B was investigated by TEM observation to clarify the microstructural effect related to this yielding behavior.

Dispersion of fine precipitates

Figure 9 shows the distribution of fine precipitates observed by TEM on a replica for a specimen of steel B annealed at 850ºC. Fine precipitates of 10 to 40 nm diameter are distributed, in which niobium and carbon were detected by EDX analysis and also nitrogen was detected in some cases. The arrays of relatively coarse precipitates seem to be the outlines of grains. It is interesting that some of these arrays of coarse precipitates accompany with the parallel precipitates arrays. In the space between this pair of arrays, fine precipitates are not observed, rendering a nearly precipitation free zone (PFZ) besides small numbers of coarser precipitates. While the so-called PFZ is formed in both sides of a grain boundary in general, these spaces with small precipitates were apparently observed to be located at one side of grain boundary.

The increase in tensile strength of steel B against steel A is approximately 30 MPa caused by both, precipitation hardening and grain refinement as shown in Figure 4. Therefore, it can be considered that the strength level of the region neighboring the grain boundary where the precipitates are depleted (PFZ) is lower compared to the intra-granular regions due to the absence of precipitation hardening, which eventually leads to the lower yield strength as schematically shown in Figure 10. However, with progressing deformation after yielding, intra-granular deformation mainly takes place and the uniform tensile strength is consistent with the intra-granular strength additionally strengthened by the fine niobium precipitates.

Mechanism of PFZ formation during annealing

The niobium carbides in the chemistry of steel B, 0.0052%C and 0.068%Nb, must be fully precipitated after hot coiling at 640ºC according to the solubility of niobium carbide in ferrite derived by Turkdogan [7]. Therefore, this higher amount of fine niobium precipitates is expected to retard the recrystallization during annealing and the grain growth is also suppressed by their pinning effect. It is considered that the depletion spaces of precipitates neighboring to the grain boundaries are formed during the grain growth after recrystallization because the shape and location of this space is in close proximity to those of the recrystallized grain boundaries, as previously mentioned.
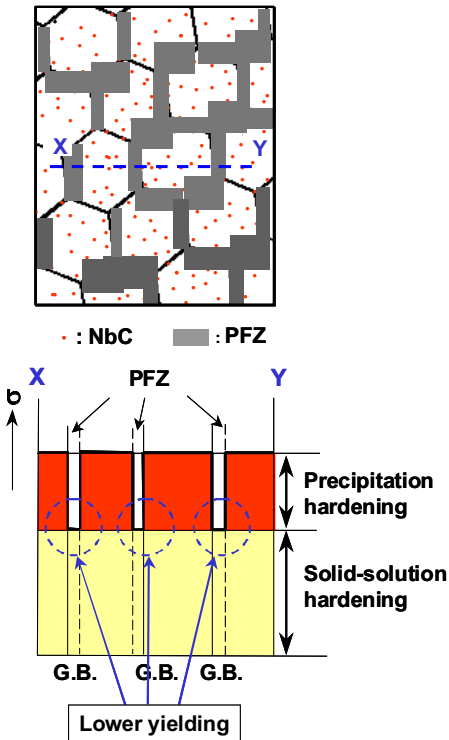
Figure 9. TEM image with replica and EDS spectra of precipitates observed in the annealed sheet at 850ºC of steel B.
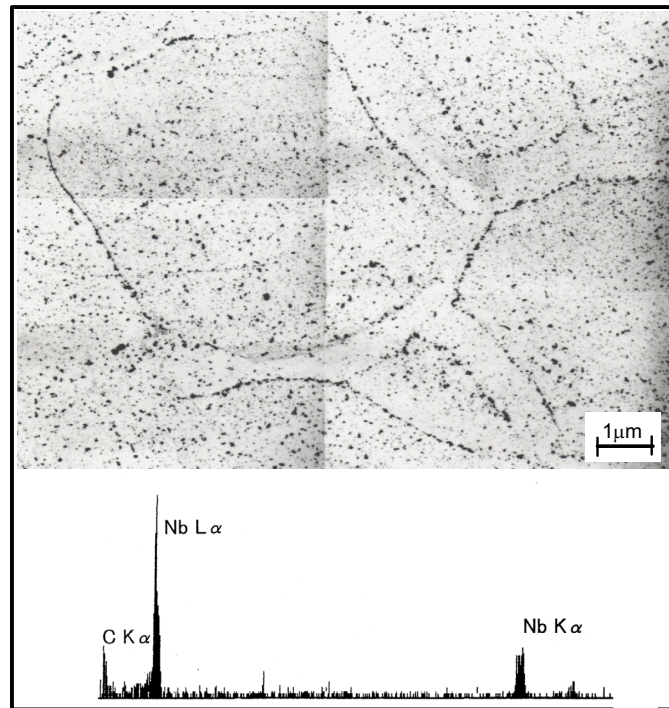
Figure 10. Schematic illustration showing inferred mechanism of lower yield ratio in the developed steel (steel B).

The hypothesis with respect to the formation of these precipitate-depleted-zones during annealing in case of steel B is schematically shown in Figure 11. At the lower temperature above the recrystallization temperature, TR, the grain boundary of recrystallized grains is restrained by the pinning effect of fine niobium precipitates having diameters of around 10 nm. Elevating the annealing temperature tends to coarsen the fine precipitates by the Ostwald-ripening, where the grain boundary is a predominant site because of its larger diffusivity of niobium compared with the volume diffusion. Coarsening of precipitates on grain boundaries relieves the pinning force and give rise to the grain boundary migration. Therefore, it is inferred that the arrays of coarse precipitates parallel to the grain boundaries as shown in Figure 9 show the trace of the previous position when the grain boundaries started their migration. Once the grain boundary reaches the adjacent fine precipitates in the grain, the coarsening of precipitates is accelerated due to the increase in diffusion rate of niobium by changing from volume to boundary diffusion. However, the equilibrium solubility of niobium carbide during annealing at 830 to 870ºC is particularly small, i.e., 3 to 8 ppm in carbon content. It is indicated that a proceeding grain boundary migration leading to lower amounts of precipitates in the PFZ might cause the sweeping effect by the grain boundary. Therefore, the coarsening and the solution of niobium precipitates take place together with the grain boundary migration, which consequently leads to the formation of the unique precipitates-depleted-zone only in one side of grain boundary.
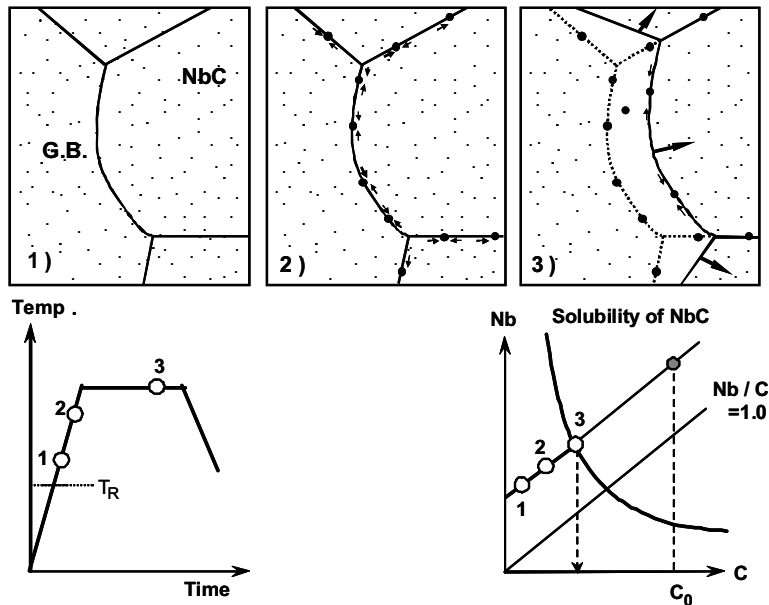
Figure 11. Schematic illustration showing the hypothesis with respect to the mechanism of the PFZ formation in steel B.

Effect of the PFZ morphology on yield strength [8]

As described above, it is inferred that the formation of PFZ results in the lower yielding which starts from the softer PFZ neighboring the grain boundary in the initial deformation stage. In order to clarify this hypothesis, the morphology of PFZ was changed to investigate the effect of PZF on yield strength.

Table II shows the chemical composition of steels used in this study. Hot bands were cold-rolled to 0.65 mm gauge and annealed with several heating conditions in the laboratory. Cold-rolled sheets were annealed at 850 °C for 60 s in the infrared furnace with heating rates from 2°C /s to 15 °C/s. The annealed sheets were skin-pass rolled with an elongation of 0.5%. These specimens were subjected to tensile testing and microstructural observation by optical microscopy and transmission electron microscopy (TEM). The volume fraction of PFZ was determined by measuring the area fraction of PFZ. TEM observation was also carried out on the deformed specimens in order to correlate tensile properties with the PFZ.

Table II. Chemical composition of steel used (mass%).

C	Si	Mn	S	Sol.Al	N	Nb
0.0068	0.02	0.99	0.009	0.052	0.0025	0.101

Figure 12 shows the effect of the heating rate on the mechanical properties of the specimens annealed at 850°C for 60 s. The yield strength considerably decreases when reducing the heating rate, while the tensile strength remains constant. Figure 13 shows the optical micrographs of the specimens annealed under heating rates of 2°C/s and 15°C/s. There is no obvious difference in the ferrite grain size between these specimens. This indicates that the clear decrease in yield strength with reducing the heating rate cannot be explained from the Hall-Patch law.
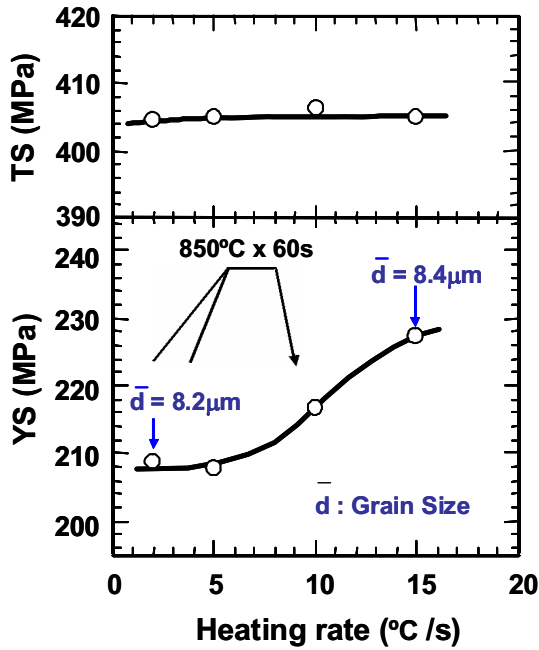
417

Figure 12. Relationship between mechanical properties and the heating rate in the specimens annealed at 850ºC for 60 s.
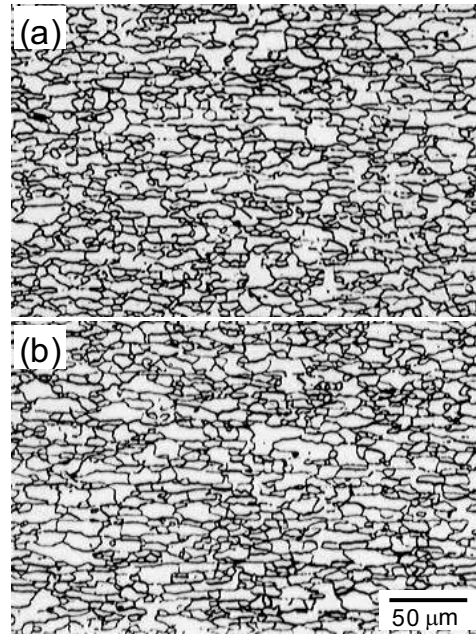

Figure 13 Optical micrographs of the specimens annealed with the heating rate of (a) 2ºC/s and (b) 15ºC/s.

Figure 14 shows TEM micrographs of the annealed specimens with heating rate of 2ºC/s and 15 ºC/s. The PFZs were observed in the vicinity of grain boundary in both specimens. However, both the width and the frequency of the PFZ are much larger in the specimen annealed at the lower heating rate. Figure 15 shows the effect of the volume fraction of the PFZ on the yield strength and n-value. The yield strength decreases and the n-value increases significantly with increasing volume fraction of PFZ. Therefore, it could be inferred that the PFZ is the dominant factor for the yielding and work hardening behavior in this grain-refined IF steel.
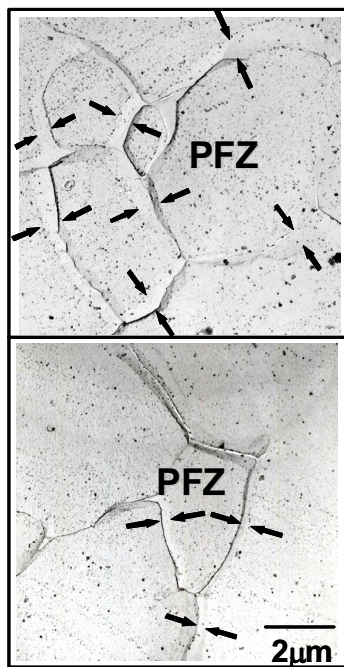

Figure 14. TEM micrographs with replica of the annealed specimens with the heating rate of 2ºC/s (top) and 15ºC/s (bottom).
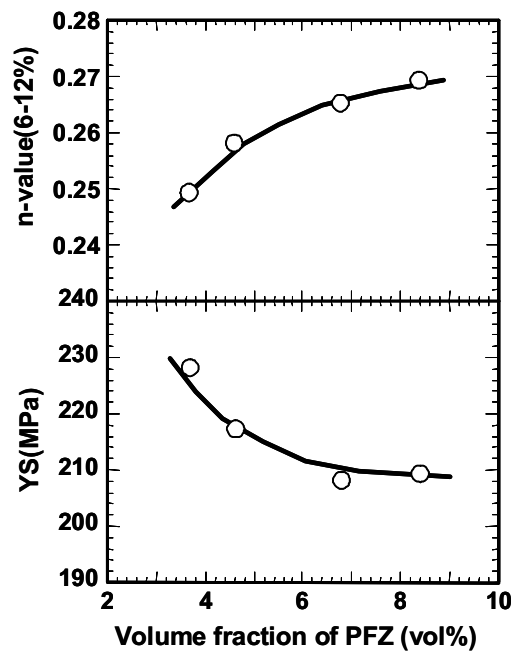

Figure 15. Effect of the volume fraction of PFZ on mechanical properties of annealed specimens.

Interaction between PFZ and dislocations during deformation.

In order to clarify the effect of PFZ on the yielding and the work-hardening behavior, deformed specimens with a tensile strain of 0.5 and 12% were subjected to TEM observation. Figures 16 and 17 show the results.
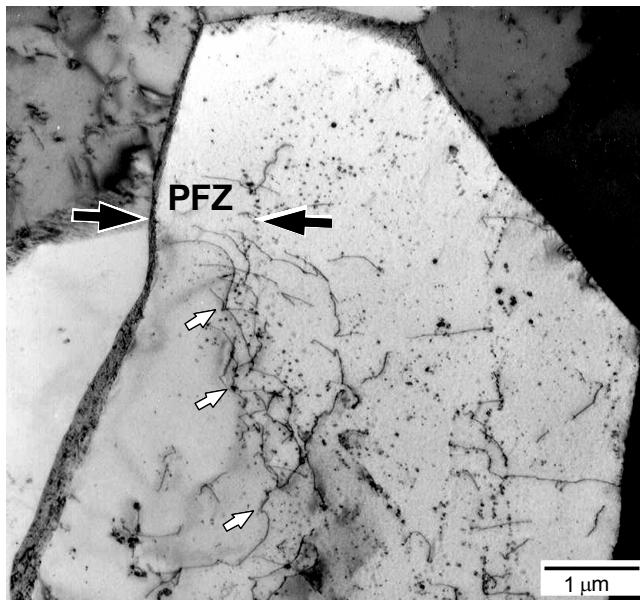

Figure 16. TEM micrograph of specimen annealed with the heating rate of $2 \,^{\circ}\text{C}/\text{s}$ and deformed with 0.5% tensile strain.
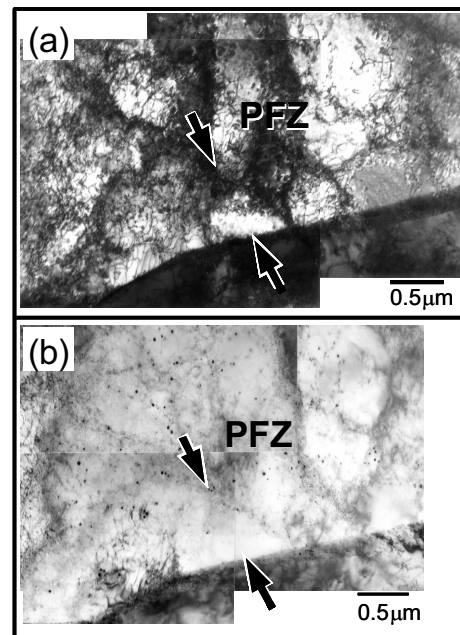

Figure 17. TEM micrographs of specimens annealed with the heating rate of 2ºC/s and deformed with 12% tensile strain. (a) and (b) show the same area with different tilt angles.

In the early stage of deformation, Figure 16 shows the TEM micrograph of the specimen annealed with 2ºC/s and deformed with 0.5% tensile strain, in which the yielding has just occurred. It has been observed that the dislocations are pinned by NbC precipitates at the boundary between PFZ and precipitated matrix (herein after referred as PFZ-matrix boundary), and they bow from the grain boundary side to precipitated matrix side as shown with the white arrows. It is also found that the dislocation density is very low in the PFZ. Since the grain boundary is considered to act as one of the effective F-R sources, it is suggested that the dislocations generate at the grain boundary and move to the precipitated matrix through the PFZ. Furthermore, the PFZ should be the softer region than the region where the NbC particles disperse homogeneously. Therefore, it is inferred that the dislocations can easily generate at the grain boundaries accompanied by PFZ. This could be the reason why this steel exhibits lower yield strength than the conventional IF-HSS and the yield strength of this steel strongly depends on the volume fraction of the PFZ.

Figure 17 (a) and (b) show the TEM micrographs of the specimen annealed with 2ºC/s and deformed with 12% tensile strain, where the flow stress comes closer to that in the specimen annealed with larger heating rate. These micrographs show the same area with different tilt angles in order to observe the relationship between dislocation morphology and NbC precipitates distribution. At this higher tensile strain, uniform dislocation cells are observed over the whole grain and no obvious difference in the dislocation morphology has been observed between the matrix and the PFZ location. Since the dislocation cell structure would be the dominant hardening structure in this higher strain region, the PFZ would become less effective as a site for

419

the dislocations to generate or accumulate. It is inferred that this is the reason why the n-value decreases and the flow stress restores in the higher strain region than 12%.

Secondary Work-Embrittlement [9]

In general, IF steels have low grain boundary strength in comparison to intra-granular strength because interstitial elements do not exist at the grain boundaries. In particular, in high-strength steels based on IF steel, it is necessary to consider measures to prevent the secondary embrittlement caused by the strength difference between the grains and grain boundaries. Therefore, anti-secondary work embrittlement was investigated in the new 440 MPa grade fine grain IF steel. This was compared with the conventional titanium bearing IF high strength steel sheet. Furthermore, the effects of both grain refinement and boron addition on the improvement of anti- secondary work embrittlment in IF steels [10] were compared.

Experimental Procedures

The materials with the chemical compositions listed in Table III were melted and cast in the laboratory. Steels A00 through A15 show the typical chemistry of the conventional ultra low carbon titanium bearing IF steel, where the base solid-solution strengthening elements are common as 0.3%Si, 2.0%Mn and 0.075%P and boron content is varied from free to 15ppm. In Steels B00 through B15, the carbon and niobium contents are consistent to the basic alloy design of the grain-refined IF-HSS in order to apply grain-refinement and precipitation strengthening by NbC precipitates, where the base solid-solution strengthening elements are common as 0.01%Si, 2.0%Mn and 0.08%P.

Table III. Chemical compositions of steels investigated (mass%, *: ppm).

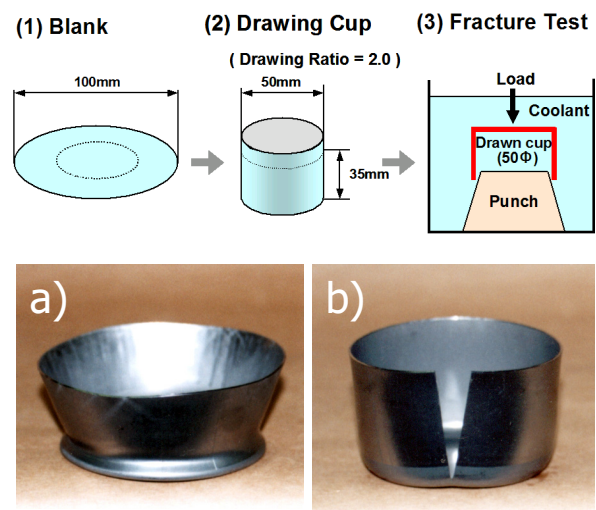| Steel	C*	N*	S	Nb	Ti	B*
A00	24	18	0.005	0.004	0.045	tr.
A02	26	18	0.005	0.003	0.045	2
A04	26	17	0.005	0.004	0.045	4
A08	21	19	0.005	0.004	0.046	8
A15	20	19	0.005	0.003	0.045	15
B00	60	30	0.006	0.11	tr.	tr.
B02	66	26	0.006	0.11	tr.	2
B04	59	24	0.006	0.11	0.001	4
B10	54	26	0.005	0.10	0.001	10
B15	58	25	0.006	0.11	0.001	15

Figure 18. Schematic diagram of evaluation method of the transition temperature for secondary-work-embrittlement. (a) non-brittle fracture, (b) brittle fracture.

The ingots were hot-rolled into the intermediate size of 30 mm thick. After soaking at 1200ºC for one hour, they were hot-rolled to 3.0 mm thick with the finishing temperature at 890ºC followed

by air-cooling. In order to simulate the hot coiling, hot bands were soaked at 620ºC and 580ºC in steel A and B series respectively for one hour followed by furnace cooling. After pickling, hot-bands were cold-rolled to 0.75 mm gage with a rolling reduction of 75%. These cold-rolled sheets were annealed at 795ºC and 825ºC in steel A and B series, respectively for 110 s using salt bath. Subsequently, they were subjected to skin-pass rolling with an elongation of 0.5%. Tensile tests were carried out using JIS No.5 specimens in transverse direction. The r-values were measured as described above. The transition temperature of secondary work embrittlement was evaluated by flanging test of drawn-cup with the cup-height of 35 mm and the drawing ratio of 2.0 schematically shown in Figure 18.

Mechanical properties of 440 MPa grade IF-HSS

Figure 19 shows the effect of the boron content on the tensile properties in both the conventional and the grain-refined IF-HSS. The tensile strength in both types of steels is almost on the same level of 450 to 460 MPa. However, the yield strength of steel B series is 15 to 20 MPa below that of steel B series, which is reflected by the formation of unique PFZ. Mean r-values of steel B series are higher than those of steel A series, which is enhanced by an increasing boron content. Steel B series exhibits more desirable tensile properties of higher r-values and lower yield strength for stamping exposed panels in view of deep-drawability and surface reflection, which is maintained even under the boron bearing chemistry.
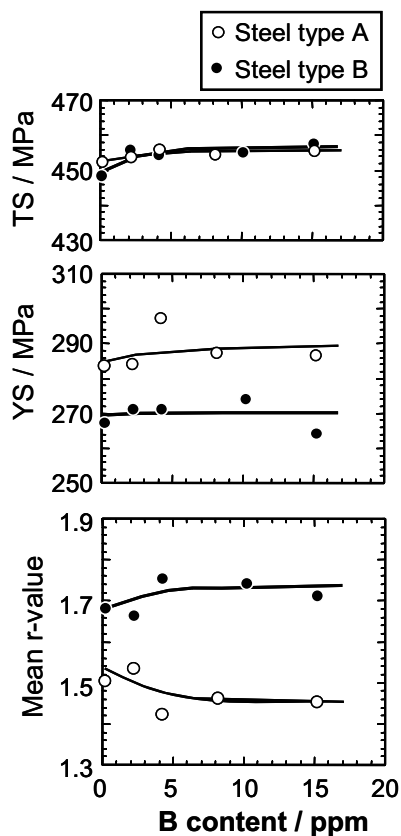

Figure 19. Effect of B content on tensile properties of the annealed specimens in steel A and B series
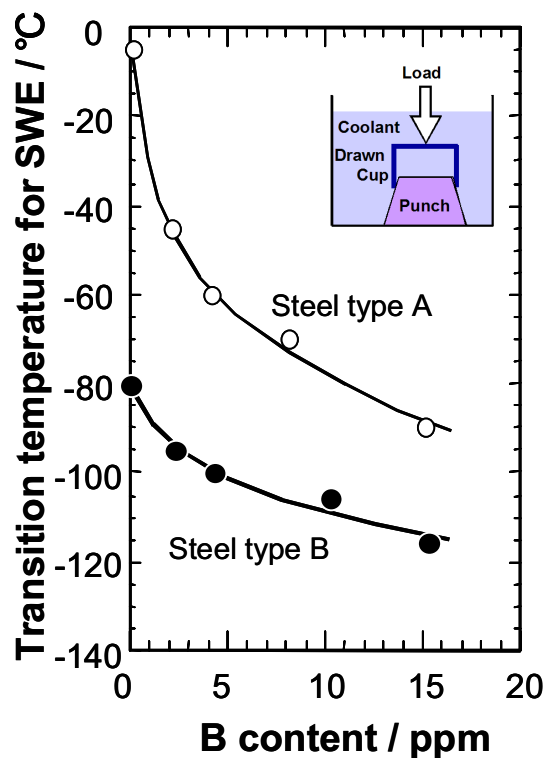
Figure20. Effect of B content on the transition temperature for secondary work-embrittlement.

Secondary work-embrittlement

All of the fractured surfaces in this study were the inter-granular surfaces. Figure 20 shows the effect of the boron content on the transition temperature (Tc) for secondary work embrittlement

(SWE). The transition temperatures of both steels were improved with an increasing boron content in the steel. In case of a boron free chemistry, steel A00 being a conventional IF HSS, exhibited a Tc of −5 ºC, but in steel B00 representing the developed grain-refined IF HSS, Tc is remarkably reduced to −80ºC. This is equivalent to the 10 ppm boron bearing in steel type B.

Figure 21 shows the relationship between Tc and the ferrite grain size, where the tensile strength level is 450 to 460 MPa for all specimens. The grain sizes of steel B series are 7 to 8 μm and are thus smaller than those of steel A series being 10 to 11 μm. Grain-refinement is another effective method to improve the anti-secondary work embrittlement (SWE). Moreover, it is inferred that this improvement of Tc in the developed chemistry such as steel B series is attributed to the alleviation of stress concentrations near the grain boundaries during deep drawing by the existence of soft PFZs besides the grain refinement [11].

Press-Formability of Grain-Refined IF-HSS [12]

Line-up of grain-refined IF HSS, SFG-HITEN

Grain-refined IF HSS have been developed as cold-rolled steel sheets and galvannealed steel sheets based on the above metallurgical concepts for grades of 340, 390 and 440 MPa tensile strength with the typical mechanical properties listed in Table IV including the tensile properties in the transverse direction using JIS No.5 specimens, mean r-value and the transition temperature for secondary work embrittlement. Press formabilities of the developed grain-refined IF-HSS were compared to those of the conventional high strength steels by try-out-press with both the center pillar outer model and the front fender model.
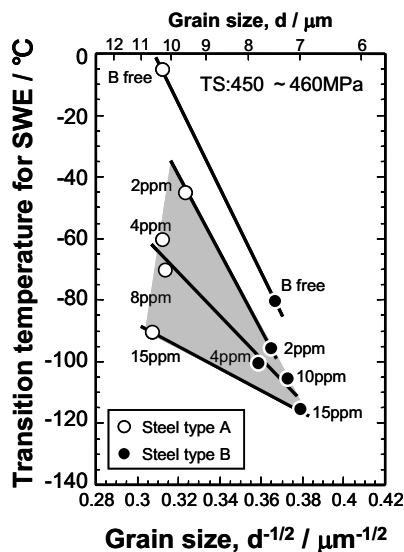

Figure 21. Relationship between the transition temperature and ferrite grain size.
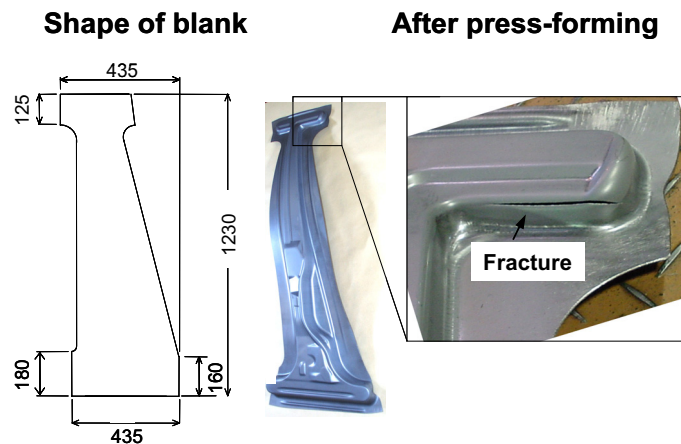
Figure 22. Shape of blank of a center pillar model and the appearance of part after press forming.

Effect of r-value against Fracture

The mechanical properties of steel sheets subjected to the try-out-press of the center pillar outer model are listed in Table V. The thickness of each material is 1.0 mm. The blank shape of the center pillar model and the appearance after press forming are shown in Figure 22. Mill oil was used as a lubricant. The center pillar outer panels were press-formed with 11,800 kN in a mechanical single-action press. The press forming speed was 10 spm. The press formabilities of

the steel sheets were evaluated as the maximum cushion force condition, in which the fracture did not take place. The fracture point in case of the center pillar outer model is indicated in Figure 22.

Table IV. Mechanical properties of grain-refined IF HSS, SFG-HITEN.

Type	Grade	Thickness (mm)	YS (MPa)	TS (MPa)	El (%)	Mean r-value	Tc (°C)
CR	SFG340	1.0	190	345	44	1.9	-100
	SFG390	1.0	235	405	40	1.9	-85
	SGF440	1.0	290	446	37	1.9	-65
GA	SGF340	1.0	197	345	42	1.7	-90
	SFG390	1.0	227	400	38	1.7	-65
	SFG440	1.0	285	442	35	1.7	-45

CR : Cold-rolled steel sheet, GA : Galvannealed steel sheet
Tensile specimen : JIS No.5, Transverse direction
Tc : Transition temperature for anti-secondary work-embrittlement with the cup-height of 35mm and the drawing ratio of cup-diameter of blank diameter, 2.1 for 340 grade and 2.0 for 390 and 440 garde.

Table V. Mechanical properties of steels used in press-forming test for a center pillar outer model.

Steel		YS (MPa)	TS (MPa)	El (%)	Mean r-value
Developed	440GA	287	440	36.0	1.75
	440GA-N	286	445	35.0	1.72
Conventional	390CR	243	402	39.5	1.62
	440CR	289	461	38.0	1.01

GA: Galvannealed steel sheet
GA-N: GA steel sheet with Ni-base inorganic lubricant film
CR: Cold-rolled steel sheet

The results of press formability tests for the steel sheets are shown in Figure23. The fracture of the conventional commercial 440 MPa grade cold-rolled steel sheet, 440CR having a mean r-value of 1.01 occurred under all of the cushion force conditions. The maximum cushion force condition applicable to the developed 440 MPa grade galvannealed steel sheet, 440GA, with a mean r-value of 1.75 was 450kN. The maximum cushion force condition applicable to 440GA-N, the developed 440 MPa grade galvannealed steel sheet with an inorganic film [13], which has the better surface frictional property than the 440GA, was 590kN. The maximum cushion force condition applicable to 440GA-N was higher than that for 390CR, the conventional drawing quality 390 MPa grade of cold-rolled IF-HSS.

Table VI. Mechanical properties of steels used in press-forming test for a front fender model.

Steel	YS (MPa)	TS (MPa)	El (%)	Mean r-value
Developed	285	442	35.0	1.70
Conventional	300	445	35.0	1.50
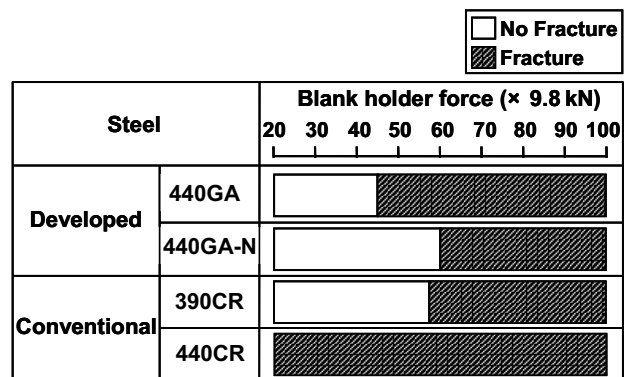
□ No Fracture
▨ Fracture

GA: Galvannealed steel sheet
GA-N: GA steel sheet with Ni-base inorganic lubricant film
CR: Cold-rolled steel sheet

Figure 23. Press-formability for a center pillar model of the developed 440 MPa galvannealed steel sheets and the conventional cold-rolled IF-HSS.

Effects of low YS and high r-value on formability

The mechanical properties of steel sheets tested in the try-out-press with the front fender model are listed in Table VI. The thickness of each material is 0.7 mm. The appearance of the front fender panel is shown in Figure 24. The conditions of press forming with the front fender model were similar to those with the center pillar outer model. The press formabilities of the steel sheets were evaluated with both the maximum cushion force condition, in which splitting did not occur and the minimum cushion force condition, in which wrinkling did not occur. The fracture and the wrinkle points are indicated in Figure 24.

The results for press formabilities of the steels are shown in Figure 25. The developed 440 MPa galvannealed steel sheet suppressed wrinkling under the lower cushion force conditions in contrast to the conventional galvannealed IF-HSS because of the lower YS, which can be expected to give less surface reflection [14]. The developed galvannealed steel sheet suppressed the fracture under the higher cushion force conditions due to the high mean r-value in comparison to the conventional galvannealed IF-HSS. Therefore, only the developed 440 MPa galvannealed steel sheet offers a formability range in the front fender model press test.
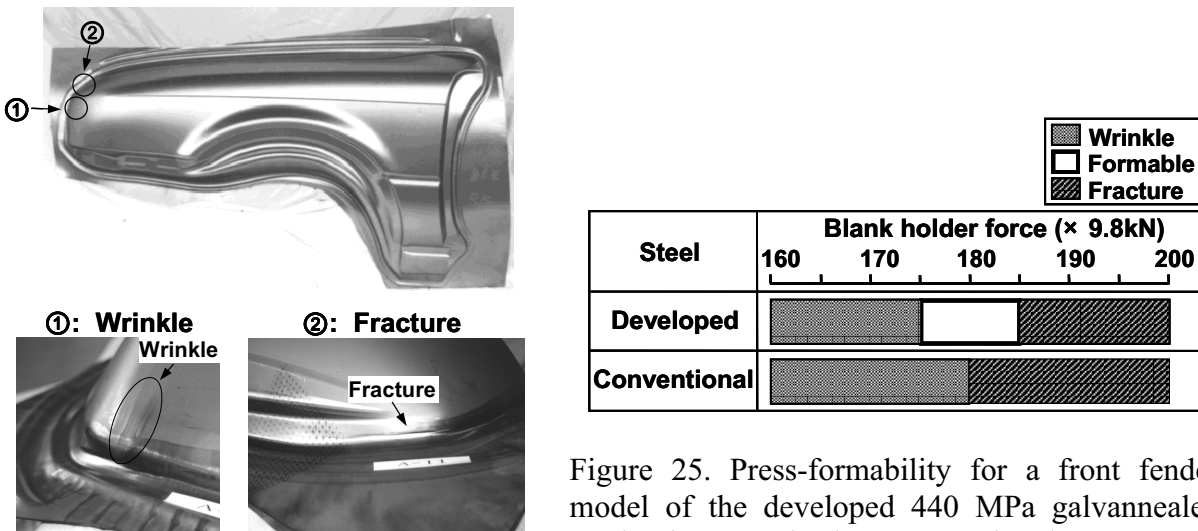

Figure 24. Front fender model to evaluate press-formability.

Figure 25. Press-formability for a front fender model of the developed 440 MPa galvannealed steel sheet and the conventional 440 MPa galvannealed IF-HSS.

Summary

A 60 ppm carbon IF steel bearing niobium was investigated to develop a new IF-HSS combining solid solution strengthening with precipitation hardening and grain refinement to improve the press formability and anti-secondary work embrittlement. The following results were obtained in view of the metallurgical features and practical performances:

1)   The increment of tensile strength in the 52 ppm carbon - 0.068% niobium bearing IF steel against the 20 ppm niobium bearing IF steel is approximately 30 MPa due to both precipitation hardening and grain refinement.

2)   The mean r-value of the developed steel was higher than that of conventional IF steel by texture development in the <111>//ND fiber in the annealed sheet. It is inferred that the improvement of texture was achieved by grain refinement of the hot-bands due to the retardation of austenite recrystallization during hot-rolling.

3)   Despite the grain refinement, the yield ratio in developed steel was lower than the conventional IF steel. It is inferred that the soft PFZ region neighboring the grain boundary preferentially yield in the early stage of plastic deformation.

4)   This PFZ preferentially forms only where the grain boundary passed during annealing. It is inferred that both coarsening of niobium precipitates and the sweeping effect by the migrating grain boundary causes the PFZ under small solubility of niobium precipitates.

5)   The grain size of the annealed sheet in the developed steel was refined to less than 10 μm, which led to the significant improvement in the anti-secondary work embrittlemnet. It is considered that the soft PFZ decrease the accumulation of strain in the vicinity of the grain boundary.

6)   As a result of mill trials to confirm the performance of the developed IF-HSS having a tensile strength of 440 MPa, the anti-secondary work embrittlement and the mean r-value were successfully improved preserving the same tensile property as in the conventional type of steel. Try-out-press trials using the developed 440 MPa grade of grain refined IF HSS exhibited an excellent press formability compared to those of the conventional high strength steel for both, the center pillar outer and the front fender models.

References

1.   Y. Hosoya, T. Urabe, K. Tanikawa, K. Tahara and N. Nishimoto, Proc. of International Symposium on Interstitial Free Steel Sheet, Ottawa, Canada (1991), p. 107.

2.   R. Pradhan, Proc. of Int. Forum for Physical Metallurgy of IF Steels (IF IFS-94), Tokyo, Japan, (1994), p. 165.

3.   L. Meyer, W. Bleck and W. Müschenborn, Proc. Of Int. Forum for Physical Metallurgy of IF Steels (IF IFS-94), ISIJ, Tokyo, Japan, (1994), p. 203.

4.   F. Kitano, T. Urabe, T. Fujita, K. Nakajima, Y. Hosoya, ISIJ Int. vol.41 (2001), p 1402.

5.   Y. Inagaki, JIM, **50**(1986), p. 250.

6.   D. A. Karlyn, R. W. Vieth and J. L. Forand: Mechanical Working and Steel Processing VII, The Metallurgical Society of AIME, New York, (1969), and p. 127.

7.   E. T. Turkdogan, Proc. of Conference on Steel Making, (1987), p. 399.

8.   Y. Ono, T. Fujita, Y. Nagataki, T. Urabe and Y. Hosoya, Materials Science and Forum, vol.426-432 (2003), p. 1481.

9.   T. Urabe, Y. Ono, H. Matsuda, A. Yoshiatake and Y. Hosoya, Proc. of Int. Forum for the Properties and Application of IF Steels (IF Steels 2003), ISIJ. Tokyo, Japan, (2003), p. 170.

10.   K. Tanikawa, Y. Hosoya and A. Nishimoto, "Physical Metallurgy of IF Steels", ISIJ, Tokyo, (1993), p. 170.

11.   W. Bleck and G. Heßling, Proc. of IF Steels 2000, ISS, Pittsburgh, (2000), p. 279.

12.   T. Urabe, F. Kitano, Y. Ono, T. Fujita, Y. Yamasaki and Y. Hosoya, JSAE 20037043, SAE 2003-01-2769, Proc. of IBEC2003, Chiba, Japan, (2003), p. 13.

13.   M. Sakurai, Proceedings of Galvatech 1998, Tokyo, ISIJ, (1998), p. 620.

14.   M. Yoshida, J.JSTP, 24-275, (1983), p. 1260.